SPEKTRUM

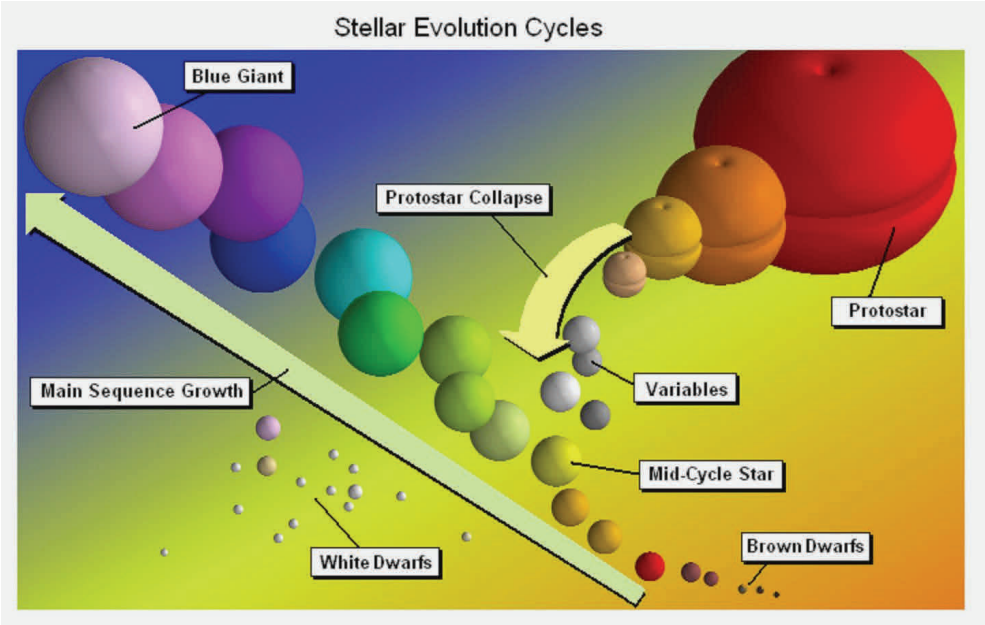

MITTEILUNGSBLATT ÜBER ASTRO-SPEKTROSKOPIE FÜR AMATEURE

HERAUSGEBER
ERNST POLLMANN
EMIL-NOLDE-STR. 12
51375 LEVERKUSEN

AUSGABE NR. 50 02/2015 ISSN 1869-4454
EINZELHEFT ALS PDF-DATEI 2,00 €

Impressum
Das Mitteilungsblatt SPEKTRUM erscheint halbjährlich jeweils im April und Oktober in der alleinigen Herausgeberschaft von Ernst Pollmann
51375 Leverkusen, Emil-Nolde-Straße 12
Redaktionelle Bearbeitung: Roland Bücke, Ernst Pollmann.
Für den Inhalt sind die Autoren selbst verantwortlich.
Titelbild: Internet, Quelle unbekannt

Kontakt
Ernst Pollmann
Emil Nolde Straße 12
51375 Leverkusen
eMail: ernst-pollmann@t-online.de
Telefon: 0214-91829

Neue Bankverbindung:
Konto Nr. 1010392019
Bankleitzahl: 37560092
Volksbank Rhein-Wupper eG, Leverkusen
IBAN: DE56375600921010392019

Inhalt Seite

RV Tauri and other post-AGB stars II. Spectra and spectral variability

by Sander Slijkhuis (sander.slijkhuis@dlr.de)

Introduction

In Paper I "Stellar evolution" (SPEKTRUM-Mitteilungen über Amateur-Astrospektroskopie Nr. 47) we discussed the evolution theory behind the formation of RV Tauri and other post-AGB stars. It was shown how evolution on the thermally pulsing asymptotic giant branch (TP-AGB) could be responsible for the dredge-up of carbon and s-process elements to the stellar surface. The extended atmosphere of these stars was discussed, as well as the predominant role of mass loss (which, in the post-AGB phase, is still largely unknown) on the evolution in the post-AGB phase.

Spectra of post-AGB stars

All post-AGB stars show supergiants-like spectra. This is because of the high luminosity (L > 1000 Lsun) and the very low surface gravity. From the outside, it may be very difficult to tell if a star is a low-mass post-AGB star, or a high-mass "real" supergiants (famous example: ε Aurigae, which used to be classified as massive supergiants but now is considered by many as post-AGB star).

There are a few properties which may hint to a post-AGB nature:

- abundances:
  if the star is carbon-rich or enriched in s-process elements it probably went through the "Third Dredge-Up" on the AGB [1] (but there are counter-examples of stars in binary systems, where mass transfer from the AGB star dumped s-process elements on the companion – this mechanism is thought to account for e.g. the "Barium" stars).
- cool (but not very cold) infrared circumstellar radiation:
  as mass-loss from the AGB stops, the dust will move away from the star and cool. Only mass loss at the AGB (and perhaps the tip of the RGB) is thought to be able to provide enough circumstellar dust [2]. Stars embedded in star-forming regions may be embedded in interstellar dust, but this is much colder. However, if the evolution is slow (which may be the case for low-mass post-AGB objects) the dust may have been dispersed so far that it is no longer observable - this might especially be an issue for low-mass post-AGB stars of spectral type A and B, which might be one of the reasons that not that many have been found).
- high-latitude supergiants:
  massive stars are born in the gas-rich disk of the galaxy and generally live not long enough to be dragged out of the galactic plane by encounters with other stars. It is also unlikely, but not impossible, that massive stars are born in gas clumps above the plane, or that they are ejected from a binary system. Thus it is unlikely that true, massive supergiants are found at high galactic latitudes. This is different for low-mass post-AGB stars which are much older. Also, post-ABG stars may be up to a factor of 10 less luminous than massive supergiants, and therefore are more near-by for the same apparent magnitude: since galactic latitude measures a viewing angle, their distance to the galactic plane is less than for a massive supergiants at the same latitude. Many post-AGB candidates have been identified this way, but note that many more may hide in the plane of the galaxy.

Several post-AGB candidates that have been identified on the basis of infrared radiation or as high-latitude supergiants seem to have an abnormal low metallicity. Using the established age-metallicity relation, these stars would be so low-mass that they never could have climbed the AGB. However, a detailed abundance analysis shows that there is a remarkable relation between

the deficiency of an atomic element and its condensation temperature [3] [4]. Elements with a low condensation temperature, such as Sulphur, have much higher abundances than elements with a high condensation temperature. Although the exact process is not understood very well (it may need a circumstellardisk to work), the accepted explanation is that elements with high condensation temperature may have deposited on dust grains nearby the cool stellar surface in the AGB phase. The dust was blown away with radiation pressure, while part of the metal-depleted gas fell back on the star. We thus have no metal-deficient, but rather a metal-depleted atmosphere. This example shows once again that stars may have properties that at first sight contradict classical views on "known" astrophysical phenomena, and that established theory is no replacement for observations (which is why we go outside and observe, even if it is cold at night).
It has been noted that post-AGB star spectra taken at low resolution sometimes seem to indicate cooler spectral types that inferred from spectra at high resolution. This has been interpreted as possible evidence for cooler circumstellarmaterial around a hotter star, where the low resolution spectra only detect the strong low-excitation resonance lines, but not the fainter high-excitation lines. While this may be true, I personally suspect that the stellar envelope is so thin that we simply see through a range of temperatures (we have no local thermal equilibrium at "the" radius of the star). Gray & Corbally, in their book [5] note that spectral classification should always be a matter of comparison to a standard taken at the same resolution and should not be confused by assuming that a spectral class has a one-to-one relationship with a physical quantity (e.g. temperature). They also note that in metal-depleted post-AGB stars the spectral type inferred from general appearance of the spectrum may look earlier than based on certain metal line strength ratios.

Spectral variability of post-AGB stars

Most, if not all, post-AGB stars show intensity and/or spectral variation. The visual variability types observed are (according to CGVS classification):

- RV Tauri
  Yellow pulsating supergiants with periods between 30-150 days. The class is defined over the light curve, which shows alternating deep minima and less deep or shallow minima. There are 3 subclasses (a,b,c) based on light curve. Independently, three spectral subclasses have been defined, which are denoted (A,B,C) see [6],[7] for a detailed description.
- SRd
  This class is a kind of collection bag for all pulsating yellow giants and supergiants with F, G, K-type spectra, amplitudes of 0.1-4 mag, and periods from 30-1100 days, excluding regular pulsators (of other variability type). The class also holds objects like the post-RGB hypergiant rho Cas.
- UU Her
  An "unofficial" subclass of the SRd stars, with some RV Tauri characteristics, consisting of high-latitude F-type supergiants; sometimes also called 89 Her stars. Also this may be an inhomogeneous class. The name-givers themselves, UU Her and 89 Her, are exceptions in that they show no s-process elements and therefore may not be post-(TP-)AGB stars.
- R CrB stars
  Carbon-rich yellow supergiants, that at irregular intervals fade away through obscuration by circumstellar dust ejection
- L, LB (Irregular)
  Another "collection bag " for irregular and slowly varying [red] giants and supergiants

All of these classes hold oxygen-rich as well as carbon-rich objects (with exception of the R CrB which are always C-rich). The above classes are for F-type and cooler spectral types. The spectral variability of the pulsating stars (i.e. not the R CrB stars) is partly due to temperature changes in the outer atmosphere, and partly due to emission lines which may be observed at various parts of the pulsation phase. But also the A-type and B-type stars usually show some variability, due to the very extended atmosphere (α Cyg type variability).
All yellow supergiants are stars that are in transition through the HR diagram, either from left to right (e.g. massive post main sequence stars) or from right to left (e.g. post-AGB stars and post-RGB hypergiants). On their way they will inevitably cross the "Cepheid" instability strip, where the H ionisation region in the envelope has a location that provides a positive feedback mechanism to small expansions or contractions, which induces the atmosphere into pulsation. The very tenuous atmospheres of the post-AGB stars make them prone to the development of non-linear pulsation effects as well. Model simulations (e.g. [8]) suggest that post-AGB stars may experience these non-linear instabilities already at lower temperatures than the classical Cepheid instability strip, and that their amplitude decrease with increasing temperature. Using public-domain ASAS light curves, Kiss et al. [9] derived an empirical instability strip for post-AGB objects.

More on RV Tauri and SRd stars

It seems that the RV Tauri phenomenon (alternating deeper and shallower minima in the light curve) occurs for a wide range of core masses and metallicities. The group of RV Tau stars seems to be quite heterogeneous [10]. There are (low-mass) RV Tau stars in globular clusters, while the field stars include both high velocity (low mass) and low velocity (high mass) stars. There are RV Tau stars with "normal" and with low metallicity (which however may be due to dust depletion as mentioned above). There are objects with a lot of cool dust and without much cool dust. And there are objects with warm dust (near the stellar surface) and without. And none of these properties seems strongly correlated with each other. However, it has been proposed that all RV Tau with warm dust are binaries [11]. Unfortunately the true luminosity of the RV Tau stars (and thereby their core mass) is not known accurately. They are too far away for parallax determination (including from Hipparcos). GAIA observations may revolutionise the insight in these stars by providing this parallax within the next few years. They do seem to follow a period-luminosity relation (with the largest periods having the highest luminosities), similar but not identical to population II Cepheids [12].

Amateur observations

Most of the recent work by professionals, such as abundance work, studies of shocks, and radial velocity measurements has been done at [very] high resolution. The faintness of these stars forces the amateur to use low resolution. At this moment I'm not yet sure at which resolution useful information may be retrieved, but without trying one won't find out. At least for long-term monitoring of the spectral variability, high resolution seems not required, but it would be good to have a link to accurate absolute fluxes, e.g. from photometry of the light curve. A fascinating possibility lies in long-term spectral monitoring, to detect temperature changes as the star moves through the HR diagram. For the lower-mass post-AGB stars the transition time may be thousands of years, but high-mass objects may have transition times as little as 100-200 years. Note that we do not expect to observe many stars in fast transition: the birth-rate of low-mass stars is much higher than that of massive objects, and stars that evolve fast will be observable only during a short time – thus statistically we mainly see slowly evolving stars. Nevertheless, several post-AGB candidates have currently a spectral type which is earlier than given by the HD catalogue [13]. Slow temperature changes are not always so obvious. For pulsating stars, it is not always clear in which phase the star was measured, and often there is some variation from cycle

to cycle. Also, spectra taken at different resolution may be difficult to compare and various authors may come to a different spectral classification. Thus, well-documented long-term observations by amateurs may still be useful.

Literature

[1] Iben, I., Renzini, A.: Asymptotic Giant Branch evolution and beyond, Ann.Rev.Astr.Astrophys.21, 271, 1983
[2] Jura, M.: RV Tauri stars as post-asymptotic giant branch objects, Astrophys.J. 309, 732, 1986
[3] Giridhar, S. Lambert, D.L, Gonzalez, G..: Abundance analyses of field RV Tauri stars.V., Astrophys.J. 531, 521, 2000
[4] Giridhar, S. et al., Abundance analyses of field RV Tauri stars. VI. An extended sample, Astrophys.J. 627, 432, 2005
[5] Gray, R.O, Corbally, C.J.: Stellar Spectral Classification, Princeston 2009
[6] Preston, G.W., et al.: A Spectroscopic and Photoelectric Survey of the RV Tauri stars, Astrophys.J. 137, p.401, 1963
[7] Pollard, K.R. et al.: RV Tauri stars - II. A spectroscopic study, MNRAS Volume 286, Issue 1, pp. 1-22, http://www.adsabs.harvard.edu/abs/1997MNRAS.286....1P
[8] Fokin, A.B.: Non-linear pulsations of the RV Tauri stars, A&A 292, 133
[9] Kiss, L.L. et al.: Defining the instability strip of pulsating post-AGB binary stars from ASAS and NSVS photometry, MNRAS 375, 1338, 2007
[10] Pollard, K.R. et al.: RV Tauri stars - I. A long-term photometric study, MNRAS 279, 949, 1996
[11] De Ruyter, S., et al.: Strong dust processing in circumstellar discs around 6 RV Tauri stars. Are dusty RV Tauri stars all binaries?, A&A 435,161, 2005
[12] Alcock, C., et al.: The MACHO project LMC variable star inventory. VII. The discovery of RV Tauri stars and new type II cepheids in the Large Magellanic Cloud, Astron.J. 115, 1921, 1998
[13] Arkhipova, V.P., et al.: Variability and rapid evolution of the protoplanetary object IRAS 18062+2410=V886 her, Astron. Lett., 33, 604, 2007

Helium in der Chromosphäre der Sonne

v. Bernd Koch

Am 15. Februar setze ich meinen BACHES Echelle Spektrografen an meinen 130mm-Refraktor, der vor dem Objektiv mit einem AstroSolar Weißlicht-Folienfilter geschützt war. Ziel des Projekts war es, den Spektrografenspalt auf den Rand der Sonne zu setzen, um in der dünnen, rund 2000 km dicken Chromosphärenschicht der Sonne, die oberhalb der Photosphäre liegt, Protuberanzen in Emission zu detektieren. Die Bildsequenz in nachstehender Abbildung ist wie folgt von links nach rechts zu interpretieren.

Spalte 1: Befindet sich der Spalt auf der Photosphäre, erscheint die Hα-Linie wie erwartet dunkel in Absorption.

Spalte 2: Schiebt man den Spektrografenspalt in Richtung Sonnenrand, so erkennt man beidseitig in den Flügeln der dunklen Hα-Linie bereits eine verbreiterte Emission; sozusagen „helle Ränder" beidseitig der schmaleren Absorptionslinie.

Spalte 3: Nun befindet sich der Spalt über der Chromosphäre ohne die störende Photosphäre. Die aufgrund von Gasbewegungen thermisch verbreiterte Hα-Linie ist deutlich in Emission zu sehen. Der Spalt liegt zudem genau auf einer Protuberanz.

Spalte 4: Weit außerhalb des Sonnenrandes ist die Hα-Linie wieder in Absorption zu sehen. Dies entspricht wieder dem normalen Tageslichtspektrum von gestreutem Sonnenlicht in der Erdatmosphäre.

Dies ist soweit ein zu erwartendes Ergebnis. Doch das Interessanteste an dieser Sequenz kommt

erst jetzt: Blickt man auf die beiden mittleren Spalten 2 und 3 der Abbildung, so taucht 4 Zeilen ("Ordnungen") oberhalb von der Hα-Linie plötzlich eine sehr helle Emissionslinie auf. Da ich mich auf die Hα-Linie konzentrierte, war ich anfangs sehr überrascht über diese Spektrallinie, deren Wellenlänge ich gut abschätzen konnte, weil sie direkt neben dem Natrium-Dublett Na D liegt. Die Kalibrierung des Spektrums ergab die Wellenlänge 5875,62 Angström. Somit ist die Identifikation mit einer Linie des neutralen Heliums sicher. Die Recherche ist spannend, hier ist das Wichtigste nachzulesen:

„Im Sommer 1868 konnte erstmals die Technik der Spektroskopie bei einer totalen Sonnenfinsternis eingesetzt werden. Aus diesem Grund reisten aus Europa einige Expeditionen nach Indien, zwei aus Großbritannien, zwei französische, eine deutsche und eine spanische. Ziel war es, das Spektrum der Sonnenatmosphäre und insbesondere der Protuberanzen zu erforschen. Wie erwartet wurden im Spektrum der Protuberanzen von verschiedenen Beobachtern helle Emissionslinien beobachtet, die auf Wasserstoff hindeuteten. Zu diesen Beobachtern gehörte auch der französische Astronom Jules Janssen (1824–1907) in Guntur. Im Gegensatz zu den anderen angereisten Wissenschaftlern blieb Janssen noch in Indien, denn er kam während der Finsternis auf den Gedanken, dass die hellen Emissionslinien der Protuberanzen auch bei normalem Tageslicht zu erkennen sein müssten, wenn man durch eine noch stärkere Auffächerung des Spektrums die Intensität des Streulichts reduzierte. Als er am nächsten Tag sein Teleskop auf den Rand der nicht mehr verfinsterten Sonne richtete, sah er seine Vermutung bestätigt, denn er konnte dieselben Emissionslinien wie am Vortag sehen, darunter auch eine sonderbare gelbe „Natrium-Linie“. Verwunderlich war, dass in den Protuberanzen ein vergleichsweise schweres Element wie Natrium vorkommen sollte, auch schien die Wellenlänge der Emissionslinie geringfügig kürzer zu sein als die von Natrium bisher bekannte.“ [https://de.wikipedia.org/wiki/Sonnenfinsternis_vom_18._August_1868]

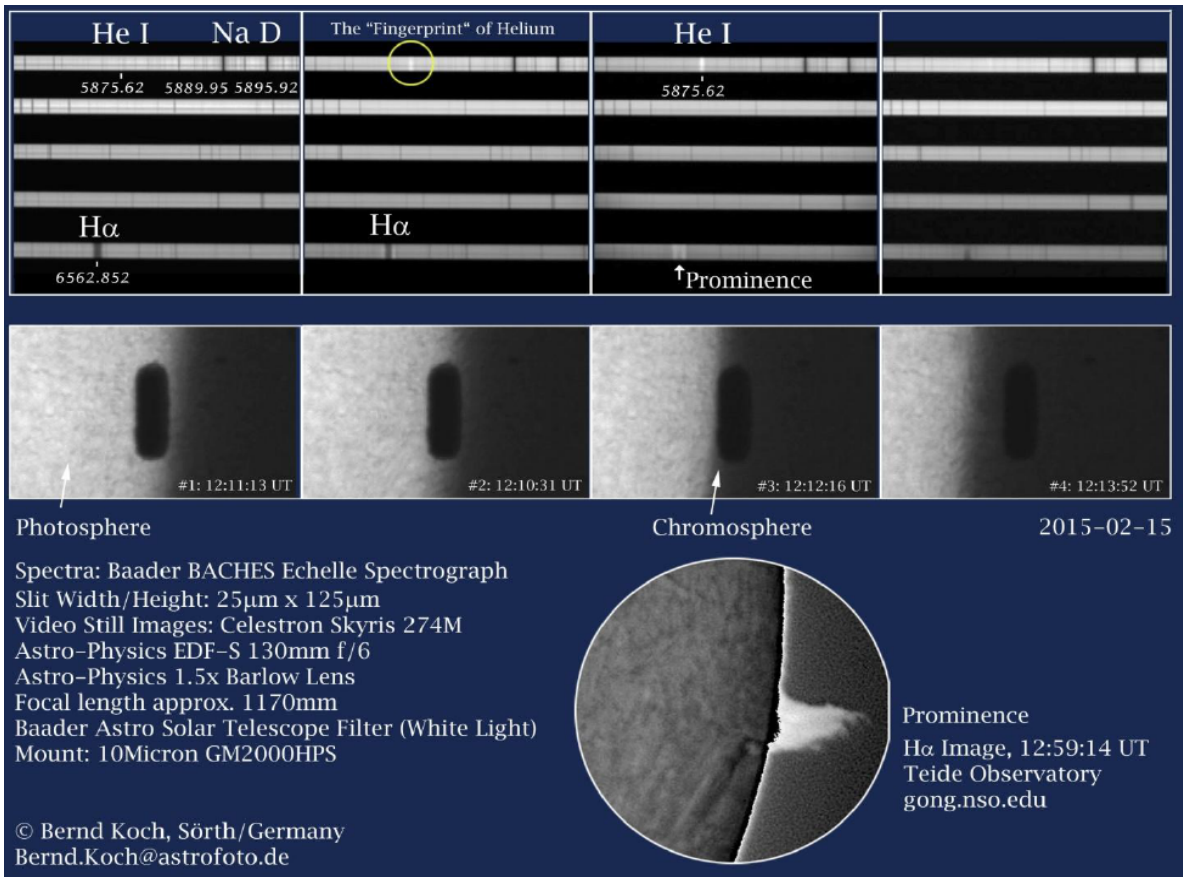

Das neue Element wurde wegen seiner Entdeckung 1868 auf der Sonne nach dem griech. Sonnengott Helios benannt: Helium. Was hier in Spalte 2 in meinem Spektrum plötzlich als helle Linie auftaucht und mich in Erstaunen versetzte, ist im Grunde das gleiche Ereignis, was zuvor Janssen 1868 passierte. Dies war also meine "rein persönliche Entdeckung" des Elements Helium auf der Sonne.

An Algorithm for Absolute Radiometric Calibration of Astronomical Spectra

Anthony Mallama (anthony.mallama@gmail.com)
Bruce Krobusek (bkrobusek@gmail.com)
Hristo Pavlov (hristo_dpavlov@yahoo.com)

Abstract

A method for modeling spectroscopic instrument sensitivity and atmospheric extinction based on observations of standard stars is described. The resulting sensitivity and extinction coefficients may then be applied as the radiometric calibration constants for computing the spectral energy in absolute units from observations of program stars. The recommended standard stars are those of CalSpec database. A listing of bright CalSpec stars having highly accurate fluxes derived from Hubble Space Telescope data is provided. Tests with observed spectra indicate that the algorithm delivered results that were accurate to about 2% under ordinary seeing conditions with just a simple grating. Strategies for successful observation and data analysis are also discussed. Under favorable conditions, observations can probably be calibrated to about 1% accuracy with the the AbsFlux algorithm.

1. Introduction

Radiometrically calibrated spectral data may be applied to a wide range of astronomical investigations. One example is variable star research where the brightness (and thus the spectrum) of an object changes over time. Calibration may either be absolute or relative. Absolute calibration results in spectral energy distributions (SEDs) with units such as ergs/centimeter^2/Angstrom/second as measured above the Earth's atmosphere. Relative calibration lacks the units of energy and, so, it might reveal whether the color of a star has changed but it cannot determine the flux in physical units.

This paper describes a precise, simple and robust algorithm for absolute radiometric calibration. Recommendations for making accurate observations and for analyzing data are also provided. Section 2 gives background information about existing computer programs that are available to the pro-am community for radiometric calibration. Most of these computer applications lack tools for absolute calibration. Section 3 describes the CalSpec library of precise spectral fluxes and explains why it is recommended for use as the reference database for absolute spectrophotometry. Section 4 examines the core of the radiometric calibration algorithm, which is named AbsFlux.

This algorithm simultaneously models instrument sensitivity and atmospheric extinction which are the two essential components of radiometric calibration. Section 5 presents the results of running the AbsFlux algorithm on simulated data for the purpose of verification. Section 6 examines the results of processing real observational data and compares calibrated SEDs to reference values. Section 7 describes the estimation of uncertainties including those found empirically from the results given in the preceding section. Section 8 discusses scenarios for successful observation and for optimal use of AbsFlux or any other radiometric calibration algorithm. A summary of the major points of this paper is provided in Section 9. The AbsFlux algorithm has been coded in a Fortran computer application of the same name. The appendix to this paper illustrates the flow of the algorithm in the source code. At the present time, the executable is a command line program controlled by parameters that are set by the user in an input file.

2. Available software

Several computer applications that are available to the pro-am community may be employed for radiometric calibration. Three widely used programs are RSpec (www.rspec-astro.com), BASS (uk.groups.yahoo.com/neo/groups/astrobodger/info) and ISIS (www.astrosurf.com/buil). These are general purpose programs which support the display and manipulation of image files, provide for wavelength calibration and output spectral profiles (pairs of wavelength and raw flux values). RSpec can process video data as well as CCD images. A fourth program, Tangra (http://www.hristopavlov.net/tangra3/) which was developed exclusively for video data, has recently been enhanced to allow for wavelength calibration. RSpec supports relative radiometric calibration, BASS seems to allow a limited form of absolute calibration, while ISIS can perform a fairly sophisticated form of absolute calibration (http://www.astrosurf.com/buil/calibration2/absolute_calibration_en.htm). Tangra now offers radiometric calibration following the AbsFlux algorithm.

Some of these applications employ the stellar spectral flux libraries developed by Pickles (1998) and the MILES data base (Sánchez-Blázquez et al., 2006 and Falcón-Barroso et al., 2011) as reference data sources for most of their radiometric computations. Both libraries are high quality resources which are used extensively in the astronomical community. The Pickles library contains 131 composite spectra that cover a wide variety of spectral types, luminosity classes and metal abundances. The MILES database is similarly rich and includes an even greater number of spectra of individual stars.

The disadvantage of using the Pickles and MILES libraries, though, is that their fluxes are normalized and thus are more appropriate for relative calibration. While the MILES spectra can be converted to absolute flux values, one must apply wide-band photometric magnitudes to the normalized fluxes at a certain wavelength. Since the magnitudes were actually derived from the spectra that process is circular. Furthermore, the MILES spectra were obtained from the ground so the normalized data itself must contain some inaccuracy due to atmospheric extinction which cannot be removed perfectly. Those are the reasons that we recommend the CalSpec library of Hubble data for high precision radiometric calibration as described in the next section.

3. CalSpec standard stars

Data obtained from above the terrestrial atmosphere with the Hubble Space Telescope is considered to be the most accurate source of radiometrically calibrated reference spectral data. The HST CalSpec database of SEDs is described by Bohlin et al. (2014). Those SED values from the Space Telescope Imaging Spectrograph (STIS) instrument on-board Hubble are the best of all.

Bohlin and Landolt (2015) validated the STIS/CalSpec fluxes by synthesizing visible and near-IR Johnson-Cousins magnitudes from the spectra and comparing them with the highly accurate magnitudes of photometric standard stars. A similar study was performed by Mallama (2015) through a comparison with Sloan magnitudes and it extended the comparison to near-UV wavelengths. Both studies indicate consistency at the 1% (0.01 magnitude) level. Since the CalSpec flux system and the two magnitudes systems were developed independently, the comparisons may be interpreted as a measure of absolute accuracy.

Most importantly, the CalSpec fluxes are given in units of ergs/centimeter^2/Angstrom/sec. Since they are not normalized, no additional information is needed in order to use the data as a reference for absolute calibration.

A list of moderately bright CalSpec stars with data from STIS between 3,000 and 10,000

Angstroms is given in Table 1. There are many fewer stars in this list than in the libraries described in the previous section. Unlike some other algorithms, though, AbsFlux does not require a dense network of standard stars. The CalSpec SEDs in the form of FITS files may be downloaded from ftp://ftp.stsci.edu/cdbs/current_calspec. Plain text files are also available from author AM.

Table 1. Recommended CalSpec standard stars for small telescopes

Name	FK5_Coordinates_J2000	Type	Mag	B-V
HD___9051_	01 28 46.502 -24 20 25.44	G7III	8.92	0.81
HD__14943_	02 22 54.675 -51 05 31.67	A5V	5.91	0.19
HD__31128_	04 52 09.910 -27 03 50.95	F4V	9.14	0.41
HD__37725_	05 41 54.371 +29 17 50.92	A3	8.31	-0.19
HD__37962_	05 40 51.967 -31 21 03.99	G2V	7.85	0.65
HD__38949_	05 48 20.059 -24 27 49.86	G1V	7.80	0.57
HD__60753_	07 33 27.318 -50 35 03.32	B3IV	6.68	-0.09
HD__74000_	08 40 50.804 -16 20 42.52	sdF6	9.66	0.45
HD_106252_	12 13 29.509 +10 02 29.90	G0	7.36	0.64
HD_111980_	12 53 15.053 -18 31 20.00	F7V	8.38	0.53
HD_116405_	13 22 45.123 +44 42 53.90	A0V	8.34	-0.07
HD_158485_	17 26 04.837 +58 39 06.82	A4V	6.50	0.13
HD_159222_	17 32 00.993 +34 16 16.13	G1V	6.56	0.65
HD_160617_	17 42 49.324 -40 19 15.53	F	8.73	0.45
HD_163466_	17 52 25.374 +60 23 46.95	A6V	6.85	0.19
HD_165459_	18 02 30.741 +58 37 38.16	A4V	6.86	0.13
HD_180609_	19 12 47.199 +64 10 37.18	F-A0V	9.42	0.15
HD_185975_	20 28 18.728 -87 28 19.94	G3V	8.10	0.68
HD_200654_	21 06 34.750 -49 57 50.28	G	9.11	0.63
HD_205905_	21 39 10.152 -27 18 23.67	G2V	6.74	0.62
HD_209458_	22 03 10.772 +18 53 03.54	G0V	7.65	0.59
BD+21_0607	04 14 35.516 +22 21 04.26	F2	9.22	0.44
BD+54_1216	08 19 22.571 +54 05 09.62	sdF6	9.71	0.48
BD+29_2091	10 47 23.163 +28 23 55.92	F5	10.22	0.50
BD+26_2606	14 49 02.357 +25 42 09.16	A5	9.73	0.39
BD+60_1753	17 24 52.268 +60 25 50.74	A0-A1V	9.65	0.07
BD+02_3375	17 39 45.596 +02 24 59.60	A5	9.93	0.45
BD+75_325_	08 10 49.488 +74 57 57.92	O5p	9.55	-0.33
HD__34816_	05 19 34.520 -13 10 36.44	B0.5IV	4.27	-0.23
HD__15318_	02 28 09.540 +08 27 36.20	B9III	4.28	-0.04
HIP_27204_	05 45 59.890 -32 18 23.16	O9.5V	5.15	-0.26
HD_214680_	22 39 15.680 +39 03 00.97	O9V	4.88	-0.21
HD_48915A_	06 45 08.920 -16 42 58.02	A1V	-1.46	0.00
HIP_23692_	05 05 30.610 +52 49 51.96	DA.8	11.78	-0.33
HIP_45880_	09 21 19.180 +81 43 27.64	sdO	11.95	-0.36
HIP_115195	23 19 58.400 -05 09 56.16	D0p	11.83	-0.30

4. Modeling atmospheric extinction and instrument sensitivity

There are two factors to consider when calibrating spectra from ground-based instruments. One is the extinction of light caused by our terrestrial atmosphere and the other is the sensitivity of the instrument itself. Models of the extinction and sensitivity functions may be derived from the observations of spectral standard stars.

Extinction is an exponential function of the air mass through which the observations are made. Therefore magnitudes are better adapted for computational work than are fluxes because magnitudes are logarithmic. Equation 1 demonstrates the relationship between magnitudes and fluxes,

$$M = -2.5 \log_{10}(F) + K \qquad (1)$$

where M is magnitude, F is flux, and K is a constant that adjusts the flux units to the zero point of the magnitude system being used.

The effects of atmospheric extinction and instrument sensitivity may appear to be unrelated but they can be represented by a single mathematical equation. Therefore, if raw spectral profiles of two or more standard stars are available, the coefficients for the models of both extinction and sensitivity may be derived simultaneously. The relationship is given by equation 2,

$$M_{ON} - M_{RN} = K_S + K_E * X_N \qquad (2)$$

where M_O and M_R are the observed and reference magnitudes, respectively, K_S and K_E are coefficients of the sensitivity and extinction models, respectively, and N indicates the serial number of the observation. The term, X, is the air mass which is represented in equation 3

$$X = \text{secant}\,(Z) \qquad (3)$$

where Z is the angle measured from zenith. This equation is for a plane parallel atmosphere. In the real case of the spherical terrestrial atmosphere it is accurate to 0.01 air mass up to 65 degrees from the zenith. Equation 2 has been presented in a variety of forms dating back to early work on the reduction of photoelectric photometry observations by Hardie (1962) and more recently by Henden and Kaitchuck (1982) and by Warner (2006). The set of N equations is usually solved by the method of least squares.

Both extinction and sensitivity depend on wavelength. So, the coefficients must be assigned to arrays indexed accordingly. After these arrays have been filled, the coefficients may be applied to the raw spectral data of program stars using the same three equations. This process results in absolute calibration.

5. Simulated data

In order to test the AbsFlux algorithm and computer code, analytical functions for atmospheric extinction and instrument sensitivity were formulated. These functions were applied to the absolute fluxes of CalSpec stars, in the inverse sense of calibration, for the purpose of simulation. Thus, the CalSpec SEDs were converted from absolute fluxes to raw fluxes. The results were then written to files of simulated raw spectral profiles.

Several stars were designated as standard stars while others were identified as program stars. The AbsFlux program read in the files of simulated raw profiles and derived the extinction and sensitivity functions from the standard stars as described in section 4. The derived functions were found to match those which had been formulated and applied in simulation.

Finally the derived functions of extinction and sensitivity were applied to the simulated raw profiles of all the stars. The computed absolute SEDs of the simulated standard stars and the simulated program stars matched perfectly with the original data from the CalSpec database.

In order to further test the algorithm, errors were intentionally introduced into the simulated spectra. For example, the profile of one standard star was reduced by 10% to mimic the effect of a thin cloud. These errors had the expected result on the SEDs of the standard stars and of the program stars.

6. Observed data

The generation and processing of simulated data demonstrated that the AbsFlux algorithm and the program logic worked correctly. Next, the algorithm was tested with real spectra obtained through telescopes. To give one example, author BK recorded spectra of ten CalSpec stars with an 8-inch telescope, an SA100 Star Analyzer grating and an SBIG ST-8 CCD camera on the night of 2015 June 24. Dark and bias frames were obtained for the purpose of image reduction along with stellar spectra. The method of accounting for non-flat field effects, which is different in grating spectroscopy than in direct imaging, is discussed in Section 8.

Inspection of the resulting images revealed that two stars had very weak spectra with low signal-to-noise ratios while a field star contaminated the spectrum of a third star. These spectra were rejected prior to processing and analyzing the remaining seven images.

The RSpec program was used to extract raw spectral profiles from the reduced CCD images. The reference features used for wavelength calibration included the hydrogen Balmer alpha, beta and gamma lines as well as the zero order star images and the minimum of the tulleric band at 7605 Angstroms. A fourth order polynomial wavelength calibration resulted in RMS residuals of less than a pixel and the dispersion of the CCD images was found to be 23.6 Angstroms per pixel. The resulting wavelength-calibrated spectral profiles are shown in Figure 1.

Next, the AbsFlux program was run to generate the coefficients of atmospheric extinction and instrument sensitivity which are plotted in Figure 2. Notice the ripples in Figures 1 and 2. These are an artifact related to the SA100 grating and the KAF sensor as discussed by Leadbeater et al. (2015a). Fortunately, the process of radiometric calibration removes the ripples.

The portion of the AbsFlux algorithm that applies the extinction and sensitivity functions to program stars had already been validated with simulation data. Therefore, when testing with real observations, all stars were treated as standards and the criterion for algorithm success was the retrieval of CalSpec SEDs from a set of spectra. The SEDs corresponding to the profiles in Figure 1 are shown in Figure 3 where they are compared with SEDs from the CalSpec library. Since two of the stars were considerably fainter than the other, they are shown at a different vertical scale in Figure 4.

Author BK also observed a smaller set of CalSpec stars on 2015 June 17. These results will be briefly summarized in the next section along with the results of video observations discussed below.

Author HP recorded spectra with a 14-inch telescope, an SA100 Star Analyzer grating and a WAT-910BD video camera on five nights between July 3 and August 13. The recording was done with the OccuRec software (http://www.hristopavlov.net/occurec/) where standard analogue video frames are stacked on-the-fly before recording the result as a higher bit depth video. Dark and bias videos were also obtained with the same exposure and gain settings. The video exposures ranged from 0.16 sec to 2.56 sec.

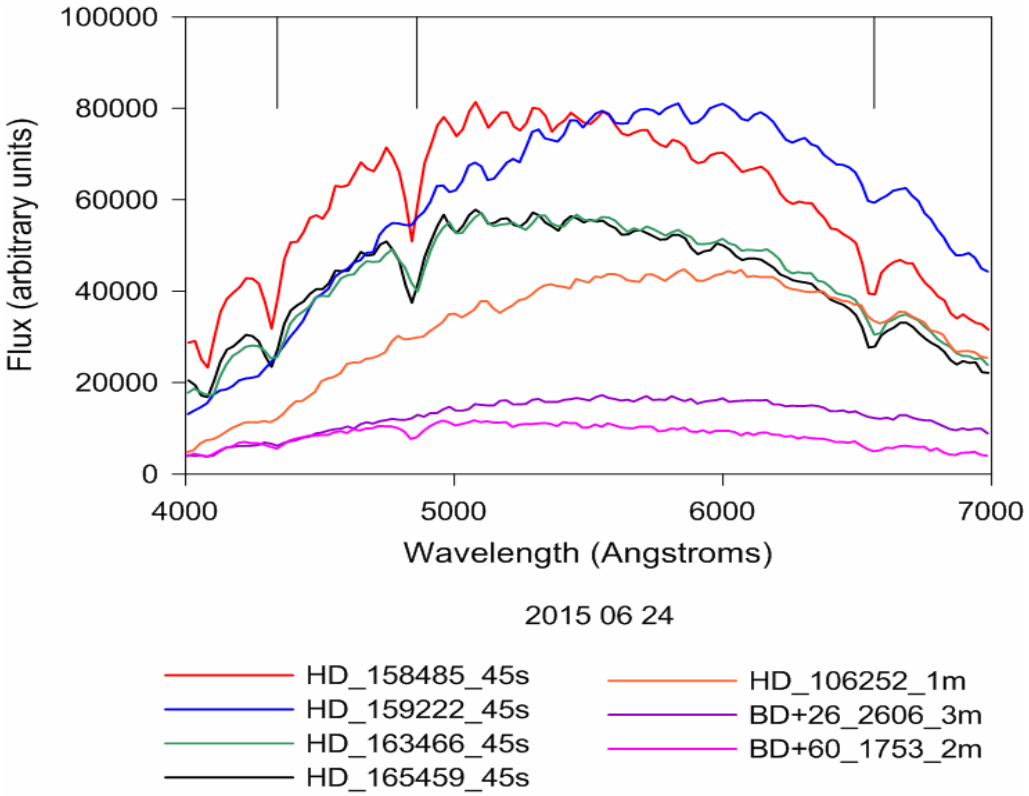

Fig. 1: The raw spectra of seven CalSpec stars with vertical lines indicating the hydrogen Balmer gamma, beta alpha lines (from left to right). Exposure durations are indicated to the right of the star names. The ripples seen here and in other spectral profiles obtained with the SA100 grating and KAF sensors are discussed in the narrative.

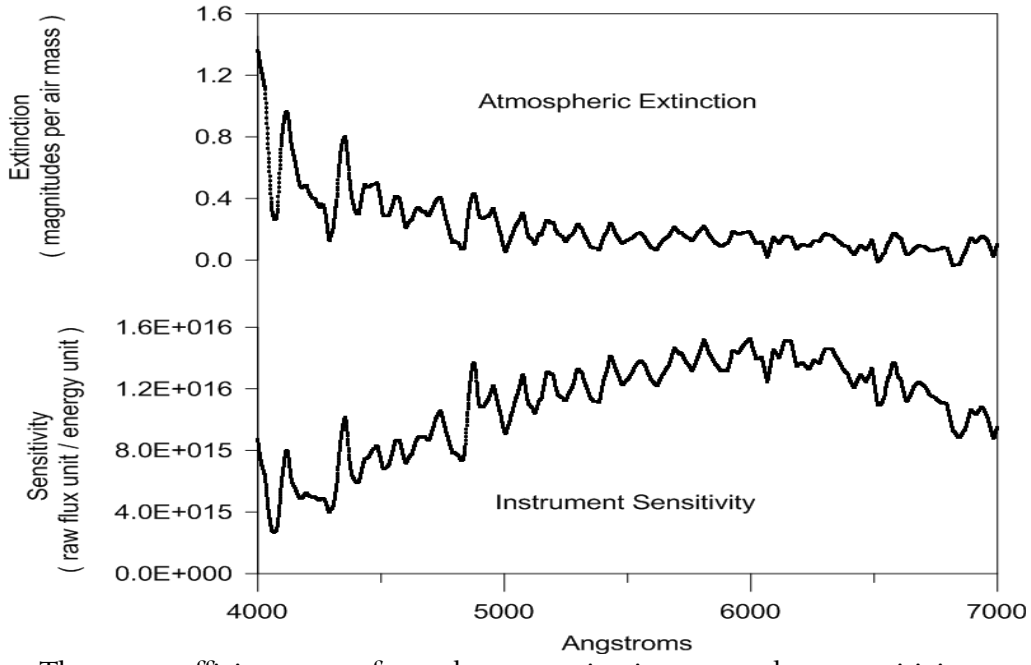

Fig. 2: The coefficients of the extinction and sensitivity model. Extinction generally decreases with wavelength. The sharp spikes between 4000 and 5000 Angstroms appear to be due to small misalignments of the hydrogen Balmer beta, gamma and delta lines. Instrument sensitivity peaks at about 6000 Angstroms in the red sensitive KAF-1600 chip of the ST-8 camera. Ripples of the same frequency as seen in the raw spectrum are revealed here too. When these functions are applied as the radiometric calibration the ripples are removed from the SEDs as shown in Fig. 3 and 4.

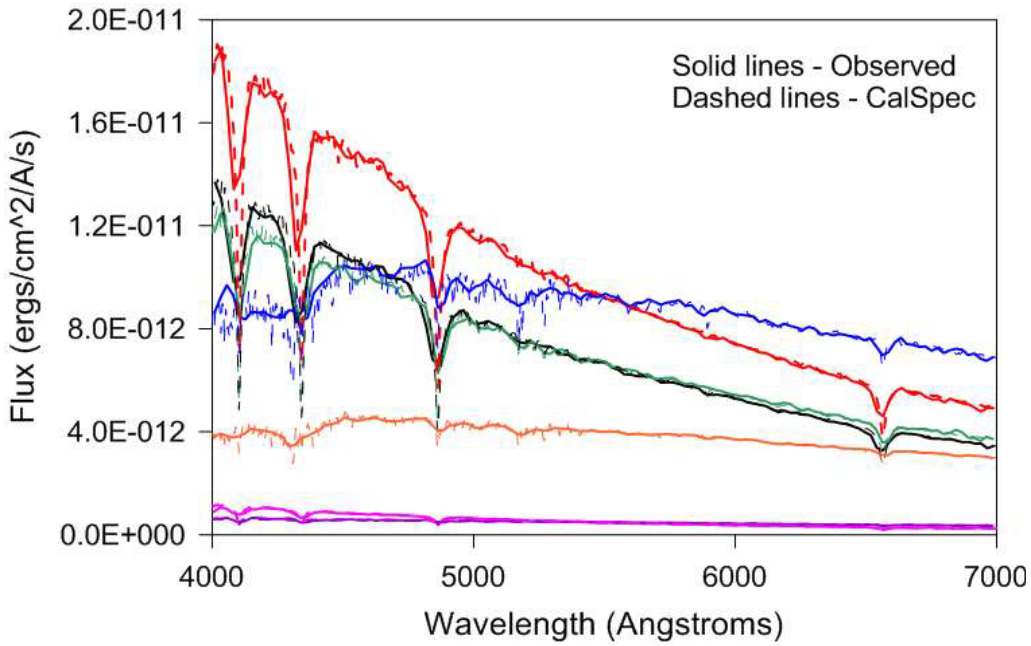

Fig. 3: Radiometrically calibrated SEDs derived from the raw spectral profiles shown in Fig. 1 are compared to those from the CalSpec reference library. The overall fit is very good though small scale differences are apparent in some of the spectral lines. One reason is that the observed spectra in this study were recorded at a much lower spectral resolution than the Hubble data. There may also be small mismatches in wavelength calibration despite performing a fourth order polynomial fit. The legend identifying the stars is the same as Fig. 1.

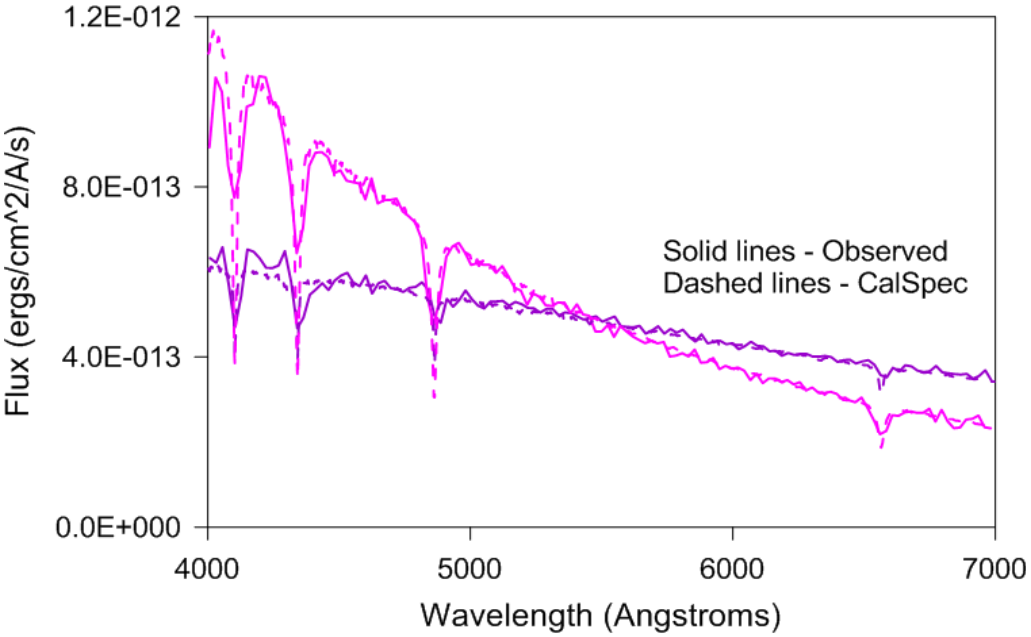

Fig. 4: The faintest two stars in Fig. 3 are shown here on an expanded vertical scale.

The reduction was done with Tangra. Between 200 and 500 video frames from the same videos were aligned using the point-spread-function of the zero order image and were then processed to produce a single spectra image using median pixel values. A sub-pixel alignment and accumulation was used during the processing. Spectral videos were corrected for dark and bias using the same exposure dark videos. Videos were not corrected for flat field effects (see Section 8). Some of the reduced spectra were then smoothened using a 1-st order Gaussian blur with FWHM of between 1 and 2 pixels. The wavelength calibration was done on a star with well

defined absorption features using the hydrogen Balmer alpha, beta, gamma and delta lines as well as the zero order star images and the minimum of the tulleric band at 7605A. A 3-rd order polynomial was fitted with RMS of less than a pixel and a dispersion of 11.6A/pixel.

7. Estimation of the uncertainty

In order to estimate the uncertainty of the observations of 2015 June 24 discussed in section 6, their mean biases and root-mean-square (RMS) differences from SEDs of the CalSpec library were computed. Table 2 lists two sets of statistics. The values under 'full_res' represent a comparison with the SEDs from the reference library at their full spectral resolution which is a few Angstroms. Since the resolution of the observed spectra was much lower (about 50 Angstroms) than those from the library, a second set of values under 'smoothed' corresponds to the differences taken after the library SEDs were averaged over the same resolution as the observations. For the full resolution comparison, the biases ranged from -0.001 to +0.017 with a mean of +0.009. The RMS values ranged from 0.032 to 0.121 with an overall RMS of 0.090. Since seven stars were observed, though, the overall error expected from the AbsFlux algorithm should be reduced by approximately the square root of the number of stars minus the number of degrees of freedom which is two (extinction and sensitivity). So that the overall reduced RMS would be 0.040. For smoothed CalSpec SEDs, the biases ranged from -0.011 to +0.012 with an average of 0.000. The RMS values ranged from 0.005 to 0.036 with an overall RMS of 0.028. When divided by the square root of 5 the overall reduced RMS value is 0.012. It is worth noting that the total exposure time used for recording spectra of the 7 standard stars was only 9 minutes. Furthermore, the observations were obtained from upstate New York which is not known for having very clear skies and the site is at an elevation of only about 200 m above sea level. Table 3 indicates that the results which BK obtained on 2015 June 17 also gave excellent results. We have found that video observations can give reliable SEDs as well. Table 3 shows the results for SEDs derived from spectra obtained by author HP from St. Clair, NSW, Australia on five nights between July 3 and August 13. In all 7 cases of CCD and video observation the absolute accuracy of the ensemble data sets are on the order of 2%.

Table 2. Residuals between star observed on 2015 June 24 and CalSpec SEDs

			--------- Differences ---------			
Star	Exposure	Air	Full_Res		Smoothed	
	(seconds)	mass	Bias	RMS	Bias	RMS
HD 106252	60	1.52	+0.003	0.032	+0.001	0.005
HD 158485	45	1.10	+0.007	0.121	-0.006	0.029
HD 159222	45	1.13	+0.017	0.057	+0.011	0.034
HD 163466	45	1.13	+0.013	0.100	0.000	0.016
HD 165459	45	1.14	+0.008	0.120	-0.004	0.029
BD +26 2606	180	1.07	+0.017	0.047	+0.012	0.036
BD +60 1753	120	1.08	-0.001	0.107	-0.011	0.034

Table 3. Residuals from all nights of observing

Date 2015	Sensor	-- Stars -- Total	Omitted	-- RMS (smoothed) -- Overall	Reduced*
June 17	CCD	4	0	0.057	0.014
June 24	CCD	10	3**	0.040	0.012
July 3	Video	7	0	0.060	0.027
July 17	Video	9	0	0.045	0.017
August 6	Video	8	0	0.053	0.022
August 10	Video	6	0	0.034	0.017
August 13	Video	13	0	0.056	0.017

* Factors in multiple observations as explained in the text
** The text explains why these stars were omitted

8. Strategies

Accurate radiometric calibration depends on the careful observations, detailed examination of the resulting images and wise usage of the algorithm for data processing. This section mentions a few useful strategies.

Flat field corrections in the usual sense are not feasible when performing grating spectroscopy. Therefore, we followed the advice of Leadbeater (2015b) and placed all the stars at the same XY pixel location of the sensors as nearly as possible. This approach causes any instrumental signatures (including vignetting and dust spots) to effect all images equally. These signatures are then modeled as part of the sensitivity function described in Section 4.

The AbsFlux algorithm models atmospheric extinction accurately over the range of air masses of the standard stars. However, calibration outside of that range is less certain. So, whenever possible, at least one of the observed CalSpec star should be higher in the sky than the programs star (or stars) and at least one CalSpec star should be lower.

For the most accurate result several standard stars should be observed over a range of air masses. If only two stars are recorded there is a danger that the calibration and sensitivity functions will fit both stars nearly perfectly even if there are anomalies in the data. (For example, with grating spectroscopy there may be a field star superposed on the spectrum of a standard star.) The same is true if three stars are recorded but two of them are at nearly the same elevation. In that case, the extinction coefficient will adjust to fit the SED of the third (possibly anomalous) star and it may not represent the true extinction. Two or more standards that are higher than the program star and two or more lower is a safe approach. One higher, one lower and one at an intermediate elevation also works well.

The program star may lie very close to a CalSpec star or may (for a time) be at nearly the same elevation in the sky. Under those circumstances atmospheric extinction dims both stars approximately equally, so absolute calibration can be achieved using just that one standard star. (The danger from anomalies as mentioned above should not be ignored though). When only one standard is observed, the AbsFlux algorithm can be instructed to ignore the effect of extinction altogether or it can apply a preprogrammed extinction coefficient in order to minimize the error from omitting empirical modeling of extinction based on the observations.

The AbsFlux algorithm outputs files containing the extinction coefficient and the instrument sensitivity function. These values should be plotted and inspected for anomalies. (See Figure 2.) Generally, the extinction coefficient should decline with wavelength from the ultraviolet to approximately 7000 Angstroms. Typical values in the blue, green and red portions of the spectrum are 0.45, 0.25 and 0.15 magnitudes per air mass, respectively. At about 7600 and 9400 Angstroms there are strong tulleric bands that can cause the extinction coefficient to increase abruptly. Sensitivity should be a smooth function that peaks in the red portion of the spectrum for most solid state sensors.

Furthermore, the AbsFlux algorithm takes spectral resolution as one of its inputs. This allows for smoothing of the SEDs from the CalSpec library in order to match that of the instrument before modeling is performed. Resolution is different than dispersion because focusing can never be perfect. The resolution may be approximated by multiplying the dispersion in Angstroms per pixel times half the width of the spectrum in pixels. The exact resolution is not too critical for successful use of the algorithm.

Lastly, it is worth mentioning that efficiency can be gained by interleaving multiple observations of the program star with those of the CalSpec standard stars. The accuracy of the radiometric

calibration should improve by averaging the program stars spectra. An even better approach is to observe multiple program stars multiple times along with the standards. In this way, accurate radiometric calibration, derived from just one set of standard stars, can be applied to a great many program stars during a single night of observing. In other words, the AbsFlux algorithm works most efficiently as a batch process.

9. Summary

This paper has described an algorithm along with a set of strategies for deriving accurate SEDs from spectral observations. The AbsFlux algorithm models instrument sensitivity and atmospheric extinction based on observations of CalSpec standard stars. The resulting calibration coefficients are then applied as the radiometric constants for computing the SEDs of program stars. A computer application which codes the AbsFlux algorithm was tested with simulated data to insure correct logical implementation. The same program was then tested with observations of CalSpec stars recorded with CCD and video cameras. Statistical analysis of the results indicates that AbsFlux produced SEDs with absolute accuracies of approximately 2%. Several strategies for achieving reliable results were described. These include positioning all stars at the same location on the sensor to minimize non-flat field effects, careful inspection of the spectral images especially for the detection of field stars that might interfere with the spectra of the target stars, observing multiple standard stars over a range of air masses which includes that of the program star or stars, and batch observation and processing of large numbers of standard and program stars.

References

Bohlin, R. C., Gordon, K. D., and Tremblay, P.-E. 2014, Publ. Astron. Soc. Pacific, 126, 711 (DOI 10.1086/677655).

Bohlin, R. C., and Landolt, A. U. 2015, Astron. J., 149, 122 (DOI 10.1088/0004-6256/149/4/122).

Falcón-Barroso, J., Sánchez-Blázquez, P., Vazdekis, A.; Ricciardelli, E., Cardiel, N., Cenarro, A. J., Gorgas, J., Peletier, R. F. 2011. Astron. Astrophys., 532, A95, 1-8. (DOI: 10.1051/0004-6361/201116842)

Field, T. 2014. Proceedings for 33rd Annual Conf. Soc. Astron. Sci. (Eds. Warner, B.D., Buchheim, R.K., Foote, J.L. and Mais, D.) 131-138.

Hardie, R.H. 1962. 'Photoelectric Reductions' in Astronomical Techniques (ed. W.A. Hiltner) University of Chicago Press.

Henden, A.A. and Kaitchuck, R.H. 1982. Astronomical Photometry. New York: Van Nostrand Reinhold.

Leadbeater, R. 2015a. Forum posting: http://www.aavso.org/first-night-out-star-analyser.

Leadbeater, R. 2015b. Forum posting: https://groups.yahoo.com/neo/groups/RSpec_Real_Time_Spectroscopy/conversations/topics/5532 .

Mallama, A. 2015. J. Amer. Assoc. Var. Star Obs. 43, 64-66. (http://www.aavso.org/media/jaavso/3075_3.pdf)

Pickles, A.J. 1998. Publ. Astron. Soc. Pac., 110, 863-878. (http://www.jstor.org/stable/pdf/10.1086/316197.pdf)

Sánchez-Blázquez, P., Peletier, R. F., Jiménez-Vicente, J., Cardiel, N., Cenarro, A. J., Falcón-Barroso, J., Gorgas, J., Selam, S., and Vazdekis, A. 2006. MNRAS, 371, 703-718. (DOI: 10.1111/j.1365-2966.2006.10699.x)

Warner, B.D., 2006 A Practical Guide to Lightcurve Photometry and Analysis. New York: Springer.

Appendix - The AbsFlux Algorithm

Note: Parts 3, 4 and 8 pertain to simulation. So they may be ignored for the purpose of processing observed spectra.

Part 1. Initialize

Input the following –

- *Site coordinates*
- *UT date*
- *Path to CalSpec master file*
- *UT time and exposure duration for each spectral profile*
- *Spectral resolution (may be different than dispersion per pixel)*

Compute JD, Greenwich sidereal time at JD and sidereal time at site.

Part 2. Input coordinates, wavelengths and fluxes of the CalSpec stars

Build the path-plus-file-name of the CalSpec master file and open the file.

Loop over the master file records which are one per star.

- *Read the star name, star file name, RA and Dec from the master file.*
- *Apply precession to the coordinates.*

Build the path-plus-file-name of each CalSpec star file.
Loop over the star file records.
Read wavelengths and fluxes from CalSpec star files.
Interpolate values to one-per-Angstrom array of fluxes.

Part 3. Simulate standard stars
Skip to part 5 if simulation is not specified.
Assign the half-width based on simulation wavelength spacing specification or spectral resolution.
Loop over standard stars.
Build the path-plus-file-name of each standard star file and open the file.
Match standard star to CalSpec star and store its number as an index.
Compute the air mass.
Loop over the specified wavelengths according to spacing specification.
Stagger the starting wavelengths for realism.
Use half-width to sum fluxes from CalSpec star.
Adjust flux for exposure duration.
Adjust flux for sensitivity function.
Adjust flux for extinction function.
Write wavelength and flux to output file.

Part 4. Simulate program stars
Do the same as for simulation of standard stars beginning with 'loop over standard stars'.

Part 5. Derive extinction and sensitivity functions from standard stars
Loop over standard stars to read, interpolate and store raw fluxes, one-per-Angstrom per star.
Build the path-plus-file-name of each standard star file.
Match standard star to CalSpec star and store its number as an index.
Compute the air mass.
Loop over standard star records.
Store the wavelengths and raw fluxes.
Loop over specified wavelengths to be processed, one-per-Angstrom.
Interpolate values to one-per-Angstrom array of fluxes.
Determine the half-width for smoothing the CalSpec spectrum.
Loop over specified wavelengths to derive extinction coefficients, one-per-Angstrom.
Loop over standard stars.
Smooth the CalSpec fluxes according to the half-width.
Compute delta magnitudes for ratios of observed and CalSpec fluxes.
Derive the extinction and sensitivity coefficients, one-per-Angstrom.

Part 6. Apply extinction and sensitivity functions to program stars
Loop over program stars
Process coordinates and compute air masses.
Build the path-plus-file-name of each program star and open the file.
Loop over program star records.
Correct each flux for extinction and sensitivity.
Output the corrected flux and its wavelength.

Part 7: Assess the standard star calibrations
Initialize the accumulating variables for overall statistics.
Loop over the standard stars.
Build the path-plus-file-name of each standard star and open the file.
Initialize the accumulating variables for statistics of one star.
Loop over each wavelength/flux pair.
Compute the index to extinction and sensitivity array values.
Compute the luminosity ratio from the extinction coefficient and air mass.
Apply the extinction and sensitivity corrections.
Normalize the difference between observed and CalSpec fluxes.
Accumulate the difference and its square.
Compute the normalized mean and RMS differences for this star.
Compute the overall mean and RMS differences.

Part 8. Assess the program star calibrations (for simulation only)
Do the same as for standard stars.

Spectral Study of Comet Lovejoy C Q2 2014

(by Alfonso L. Calvente Ortiz)

Summary

Using the spectrograph DADOS with 200 l / mm and 900 l / mm gratings at home observatory of Tejina (C11), Tenerife, we obtained the visual spectrum of Comet Lovejoy at their point of closest approach to Earth. Spectral analysis allows us to cover a range between 3800 and 7500 Å. We have compared our results with the work on other comets, allowing positive identification of the elements and molecules found and has also opened up the possibility of comparatively analyzing the structure and composition of C 2014 Q2.

1. Introduction

The astronomical spectroscopy allows chemical and structural study of comets. Comets are chunks of ice itself and dust residues originating disk of dust and gas from which our solar system was formed. The study of comets is of great interest not only from the perspective of a deeper understanding of planetary formation processes of knowledge, also for the study and identification of these molecular complexes that hold biological structures of live and that one day they landed on our planet possibly through cometary impacts. Spectroscopic analysis provides us with information that surrounds and the comma following the comet nucleus.

Approaching the sun, the core substances sublime (go directly from solid to gas) due to the effects of a quick rise in temperature produced by solar radiation, this process produces spectrally countless emission lines corresponding to different molecules and chemicals involved in the process and came entirely from the cometary nucleus. In the visible spectrum, which is the wavelength range in which we work, in addition to the effects of atomic and molecular emission analyzed, we can observe the spectrum of sunlight that is reflected on the comet. This allows to study the envelope of dust and gas that surrounds and accompanies the comet and will present different absorption lines of the solar spectrum.

2. The spectrum of 200 l / mm 2014 C Q2.

The spectrum obtained from the observatory at Tejina (Tenerife) was composed by a single wall made on a C11 300seg tube with a Atik 314L + (binx2) through a spectrograph DADOS 200 l/mm (15/01/14, 23:40).

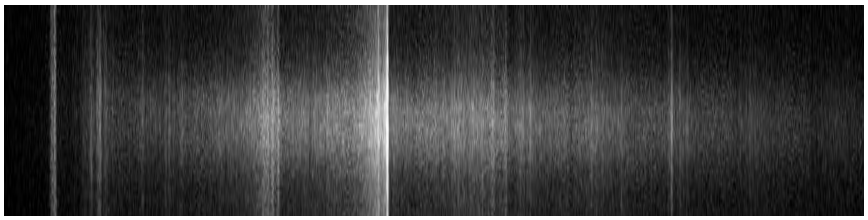

Spectrum 200 l/mm C 2014 Q2

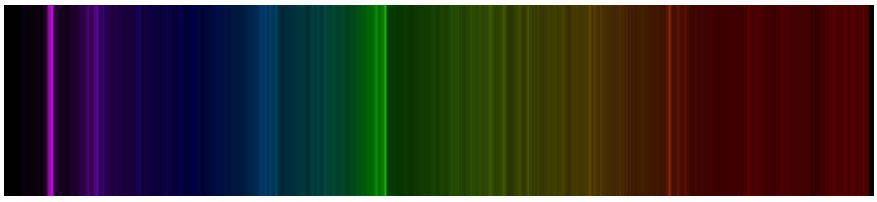

Color synthesized spectrum 200l/mm C2014 Q2

The spectrum of 200 l / mm shows a range between 3785 and 7160 Å. The raw spectrum shows a high intensity continium that corresponds to the core region of the comet, loses strength towards the ultraviolet and infrared. The strong emission lines correspond to the CN (cyanide) in the violet and C□ (Carbon diatomic) in green, somewhat attenuated the issuance of NH2 (dihydride Nitrogen - amine group) appears in red. Check the intensity of emission lines are going dissipating a greater or lesser degree depending we move away from core (in this case this distance corresponds to the top and bottom of the raw image in which the continuous and disappears), this emission can be observed even also quite far from the nucleus, and in the part of the comet's tail.

The distribution of the main lines is typical of the spectra obtained in other comets. The abundance of the identified elements is characteristic of many comets with which we visually compared the spectrum obtained. Not so much the lack of resolution as limiting the wavelength range studied, we prevent identification of the different molecules that can be found in the dust that is part of the cometary coma. We must be content with the limited analysis of the radicals identified in the visual spectrum.

Even with these limitations, we can sense the abundance of elements such as HCN, C2H2, C2H6 and NH3, every time that these same in the sublimation process produced by photodissociation those. These elements produce the radicals mentioned identified among the following:

HCN >> CN
C2H2 >> C2
C2H6 >> C2
NH3 >> NH2

To detect directly the original (and even some of the aforementioned radicals) molecules should work with radio waves or infrared and ultraviolet spectroscopy, which cover wavelengths where the detection of molecular emission lines is possible. Still very interesting analysis that can make our means. A comparison of our spectrum with the spectrum of other comets shows that both the composition and processes that are triggered in their approaches to the sun are similar:

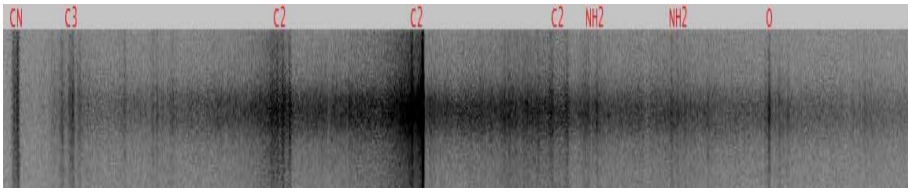

Spectrum 200 l/mm C 2014 Q2. AESESAS,2015

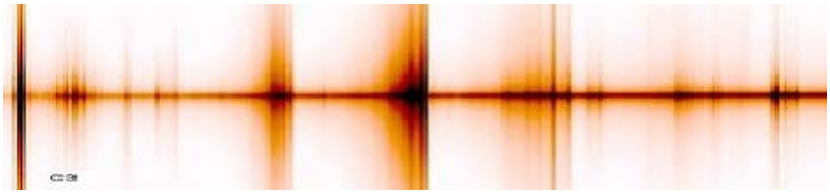

C/2002 C1 (Ikeya-Zhang)

We can see how the emission lines of comet C / 2002 C1 (Ikeya-Zhang) coincide dramatically with those observed in our spectrum of Comet C / 2014 Q2 (Lovejoy). The spectrographic analysis will allow us to identify each of the lines giving us unambiguous information on the structural composition of the core and the cloud of dust and gas that surrounds it. The chart

shown below presents the spectrum of Comet C/1995 O1 (Hale-Bopp) obtained with the 1.5 m telescope. ESO in 1997. In addition to checking the same spectral distribution, surprising detail achieved with our little humble C11 and our means against the spectrum shown in the graph.

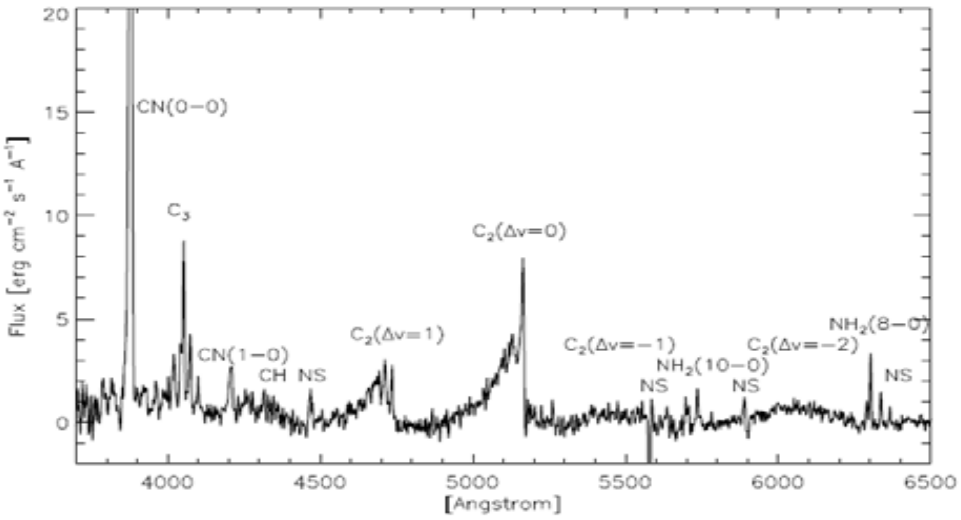

Comet C/1995 O1 (Hale-Bopp) Tel. 1,5 m. ESO 1997

A identical distribution of identified lines (more and in greater detail in our graph shown below) and matched well with the spectrum of Ikeya Zhang corroborate the common origin of these stellar objects by way of comets appear to us so close to our planet. The great cloud of Orts that surrounds our planetary system is undoubtedly a remnant of that primigenioo material that was formed our solar system.

The influence of gravitational and tidal forces, proximity or even the impact of other moving objects and can catapult new pieces of "cosmic ice" to the center of our planetary system leading to new observable comets. They keep the same general features but a deeper study of them contributes and will continue to provide important information on the processes of planet formation and even molecular structure that underpins life itself.

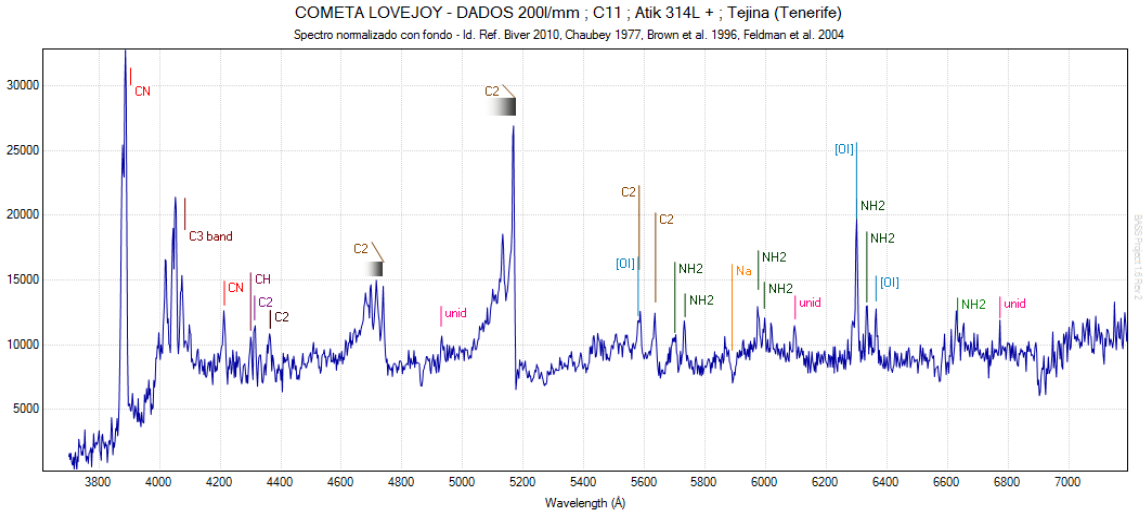

In our spectrum at 200 l / mm we have successfully identified a total of seven elements and substances:

O I: this has nothing to do with atmospheric oxygen O2 identified that exhibits strong absorption lines in the lengths of λ = 6276-6287; 6867-6884; 7594-7621 Å. Emission lines are identified within those calls forbidden transitions (only seen in some processed or molecular decomposition). In our case OI lines identified are:

λ = 6300.304 Å >> ^1D-^3P; in red
λ = 6363.776 Å >> ^1D-^3P; in red
λ = 5577.339 Å >> ^1S-^1D; in green

Oxygen responsible for emissions has been formed by different processes of decomposition of the nucleus molecules and fall off it. The original molecules are mainly H2O and CO and CO2. Other molecules that can undergo similar processes, such as HCOOH and H2CO not seem to be responsible for the OI resultant-gotten accounts that the latter do not suffer degradation fast enough to produce the transition observed in the O (^1D).

Na: In our spectrum of 200 l / mm, the reflection on Lovejoy surface of sunlight is the responsable of sodium absortion line the surface of Lovejoy. Absorption is referred to respond to the solar Na placing absocion strong doublet at λ = λ = 5889.95 and 5895.92 lines, which the resolution of our spectrograph shown as a single strong and broad absorption line. Perhaps higher resolution we can identify the issue that has been observed in other comets.

C2: two major bands found emission C2: 4737Å (-20nm) and 5165Å (-30nm). These emission bands can be found far from the nucleus, in the far tail of the comet, which implies a high production of this item.

The C2 is straightforward, mainly from C2H, which in turn comes from the decomposition of C2H2 product.

C3: The instability of this molecule difficult to study by the lack of experimental laboratory observations. Find a remarkable group between 3900 and 4140 Å, and although the density C3 lines make it very difficult to individualize, can find him lines attributable to 4700 Å.

The process leading to C3 is actually unknown. Chemically it is possible that its origin is due to the decomposition of C3H4 and C3H8, but these molecules have been detected in cometary spectra.

CN: In our visual spectrum are two CN emission bands, one of great intensity although short in 3883 Å (-4nm), and a short and very intense in 4215 Å (-4nm). The element that potentially gives rise to CN is yes HCN has been observed in the infrared, but you can not know for sure if it is the main producer or a secondary one. Festou et al (1998) concluded that seems consistent to think that the main producer of CN is the C2N2.

CH: CH has its emission peak at the 4314 Å. Its stability 1HU is very short and can range from 35-315 sec. until it is decomposed by photo-dissociation. Probably its origin is in the CH4. Methane first decay in CH2 and then east on CH. There is an emission line at 3886 Å but you can not isolate the CN at low resolution.

NH2: The NH2 from the decomposition of NH3 (newly detected radio wave). NH NH2 decay which is detectable in the ultraviolet. Nicolas Biver (Cometary Spectroscopy) presents the main lines of NH 2: 515, 545, 600, 630, 665, 695 and 735 nm. The heaviest have been identified in our spectrum.

3. The line 4133 of Bobronikoff

In 1925, from the Royal Observatory of Catania Italiano, NT<Brovonikoff takes seven shots ultraviolet camera. It is they pointed to the comet Temple-2, which achieves a visual magnitude of 9. There were seven shots with exposure times of 30-230 minutes. Brovonikoff identify the "Cyanogen" to 3883 Å, Carbon Monoxide (CO) at 4355, 4722 and 4919, and two lines for him unidentified 4133 Å and 4591 Å. 4591 Å line has subsequently been identified as among the comet C2 components, emitting at this wavelength (4590.95 Å) at the transition (2,1) R1 (61) + R2 (60).

However the 4133 Å line does not appear in the "Catalogue of High Resolution cometary emission lines" published by the "Astronomical Journal" (112, 1197-1202, 1996), which was made by ME Brown, A.H. Bouchez, H. Spinrad, and C. M. Johns-Krull.

The nearest known lines can not cause confusion since they are in 4100.30 Å (C3) and 4182.21 Å (CN). This line is not observed in the spectrum of Halley-Bopp although it seems to have formed in the spectrum of Ikeya-Zhang.

Anyway, among all the literature and consultation work we found no reference to this line or any nearby with which it might be confused. Our concern is that if on the Lovejoy.
There is a line of great intensity but it is observable in the spectrum:

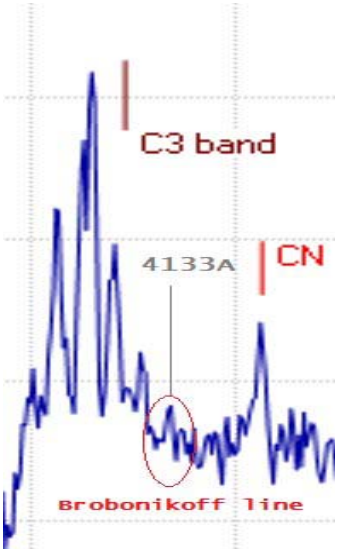

In the detail of our spectrum Brobonikoff note that the line is followed by a line relative absorption, possibly the result of sunlight reflected on the comet, and would correspond to unconjunto absorption lines where the predominant Fe I between 4132 and 4135 Å.

4. Spectrum 900 l / mm

The spectrum obtained with the spectrograph DICE with "grating 900 l/mm", the C11 tube and ccd Atik 314L +, has not allowed us a big difference in the final outcome, since we use the "ccd" with the option binx2 limiting the maximum R achievable with this grid.

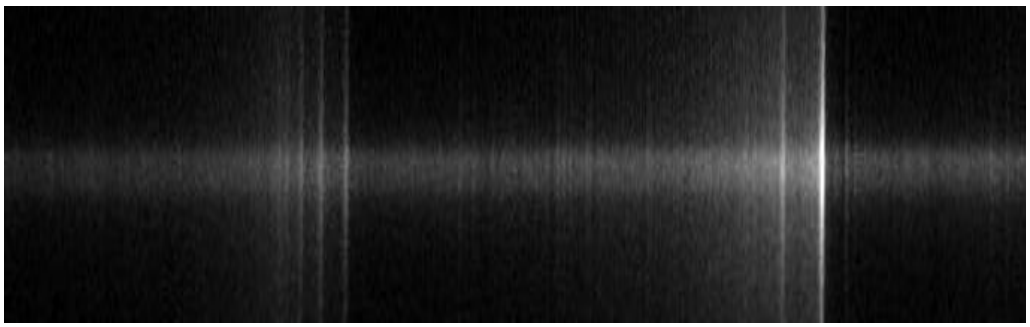

Espectro a 900 l/mm en el area de 5900-6800 Å.
La fuerte línea de emisión de la derecha corresponde al O I.

Perhaps the most revealing fact, besides the splitting of multiple lines and identifying new series of C2 emission is possible that there seems to be at the center of the absorption line of Na.

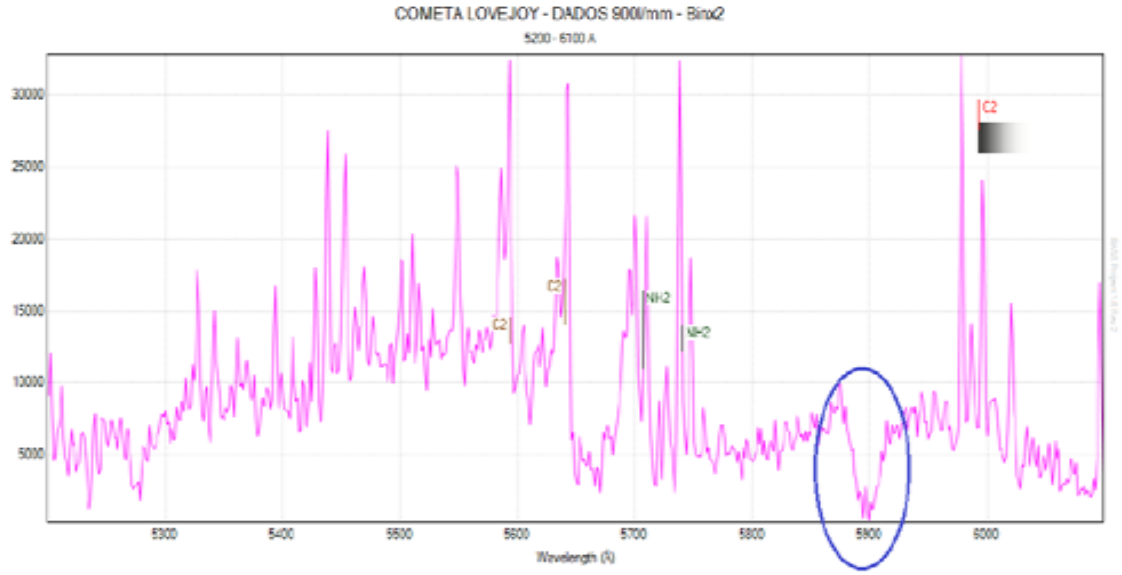

Spectrum 900 l/mm. 5200-6100 Å

5. Elements to be identified

As reference for future studies, and to confirm the importance of the study of comets has to understand not only the formation of our solar system, but to decipher the processes of molecular formation culminating developing all molecular structures that it uses life for sustenance. Huebner et al (Heat and Gas Diffusion in Comet Nuclei, 2006), shown in a comparison with the elements and molecules identified in the interstellar medium a list of those who have come to be identified in different comets and their structures:

CH NH
OH C2
CN CO
N2 CS
NS NO
N2 CH2
H2S C3
CO2 OCS
SO2 CS2
NH3 HC2H
H2CO HNCO
H2CS C2H6
CH3OCHO OH(CH)2OH
NH2 H20
C2H HCN
HN HCO
CH4 HCOOH
C4H HC3N
CH3OH CH3CH
CHCHO NH2CHO

Comparative spectroscopy with Orion Nebula

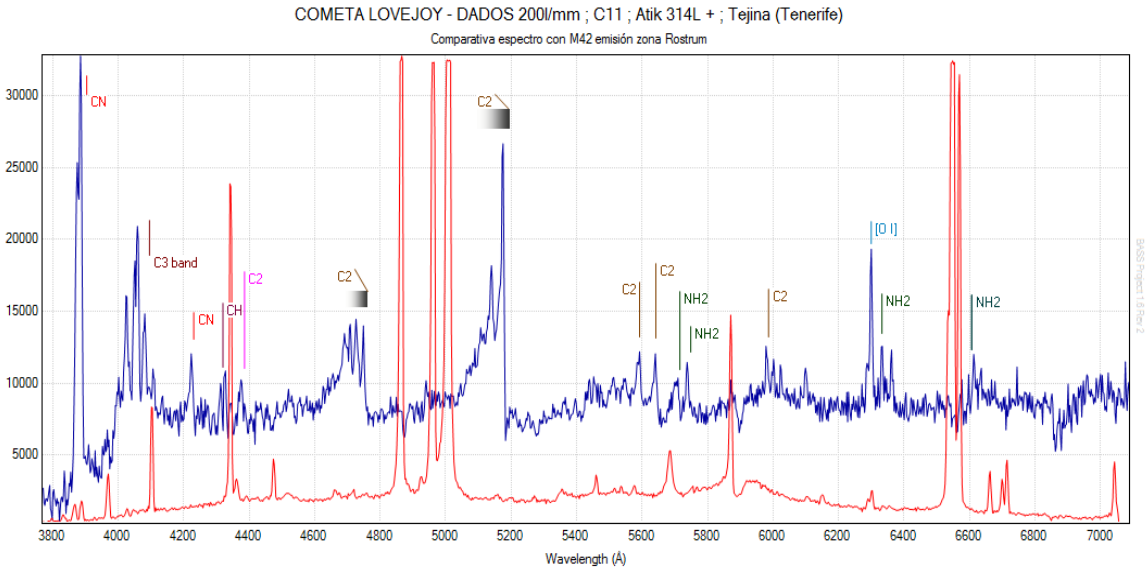

Comet Lovejoy (2015 – Blue) and M42 (2014 – Red)

In the graph we can see red spectrum of the Orion Nebula to the same resolution as the spectrum of Comet Lovejoy (in blue). It is evident that so very different spectra correspond to also completely different elements. The hydrogen cloud in which the stars in M42 are formed has a totally different molecular compounds that can identify a comet composition. The spectrum of M42 and the spectrum of a comet show two different stages of the process of star formation.

Shown in M42 we spectrum of an H II region of the cloud affected by radiation from nearby young stars that cause ionization of different nebular elements, which allows us to identification

by spectral emission in the visual. The gas we observe, then, is the same compound (region HI) who participated in training (accretion) of young stars surrounding, only now this gas been adiated and ionized significantly increasing its temperature which prevents, in that place new processes nebular collapse and accretion.On the other hand the spectrum of the comet shows the remaining compounds the end of the star formation process, ie we are in the before and after a process of star formation that runs over a period that varies depending on the size star on a scale ranging from 10 to 10 ³ million years.

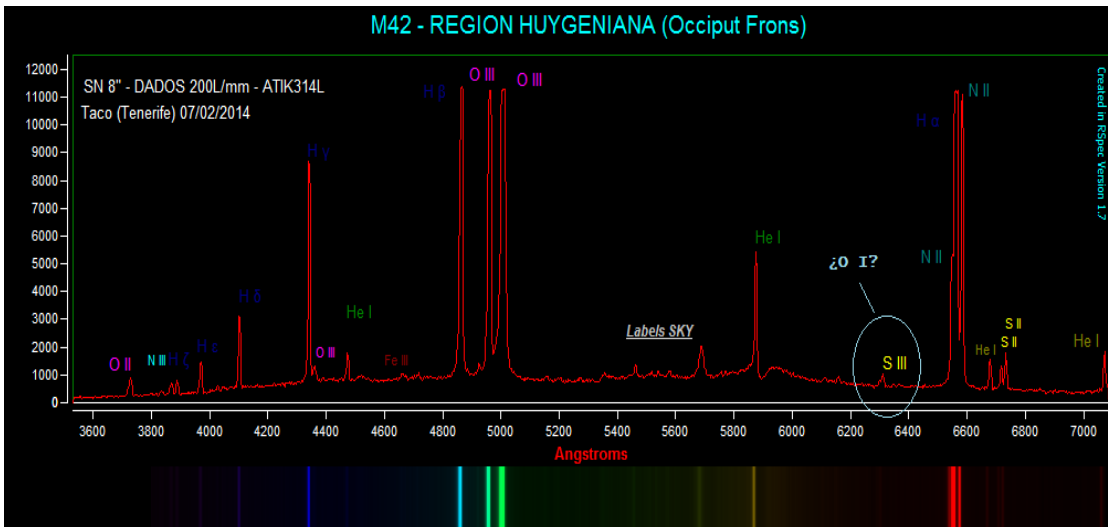

M42 spectrums with 200 y 900 l/mm DADOS done at 2014 by Calvente, Zumaquero et Sosa.

Despite not find, in general, any correlation between the lines observed in the spectrum of Lovejoy and M42 (a line coinciding appearance differs higher resolution, as HeI emission in M42 at 5876 Å that is different to that found Lovejoy at 5874.56 Å corresponding to the emission of C2), we find S III emission in M42 with a very similar to the one identified as OI in Lovejoy contour.

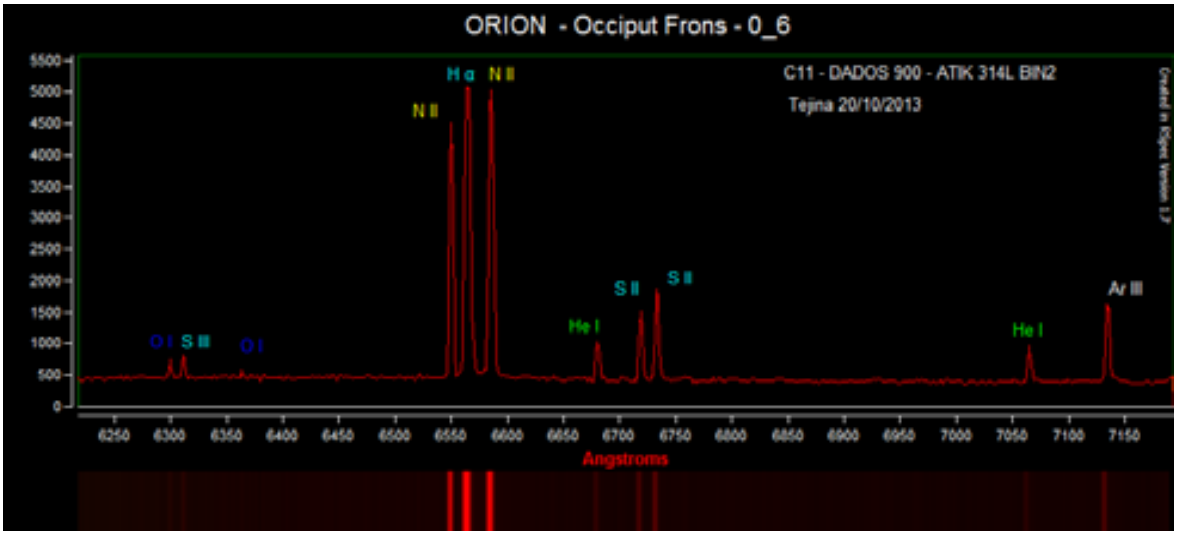

Espectro de M42 obtenidas a 900 l/mm en 2014 por Calvente, Zumaquero y Sosa

However considering the higher resolution spectrum of M42 are actually the splitting line S III also identifies a OI emission being also in the spectrum we find a splitting comet NH2 with the peculiarity that in this case the OI emission is much more intense.

It is important that information which indicates that the processes leading to the issuance of OI (forbidden line) by dissociation of more complex molecules were present in the H II region and comets radiated by our sun. However while different molecules originating in each case the process of emission from ionized oxygen is the same (transitions electronos levels are the same).

Conclusions

The media of today are arranged at the amateur level are really amazing. Not only in terms of tools and equipment with which to work in astronomy, and more specifically in astronomical spectroscopy, but also in a way unimaginable for a scientist fifty years with regard to access to specialized documentation libraries, databases, experimental simulation programs and catalogs.

All this makes our task amateur simple, an exciting trip to the intricacies of cutting-edge science spectrograph. We have checked with our own means as comets are carriers of complex molecules that constitute the fundamental building blocks of the building of life for their livelihood uses.

The discusivo study on the identification of emission lines opens the door for further study of comets, their classification, and why not, in the identification of new lines and elements such as open question Bobronikoff line. The actual magnitude of comets for the spectrographic technique is much less than the visual as this decreases to disregard the brightness of the entire object but the line or points of light from which it obtains the spectrum.

That will force us in other studies to make presentations more time we can provide light spectra at high resolution. The first brick is laid. It will be interesting to continue comparative studies with interstellar medium, accretion disks, protostars, protoplanetary disks and laboratory studies to continue watching the hands weaving life.

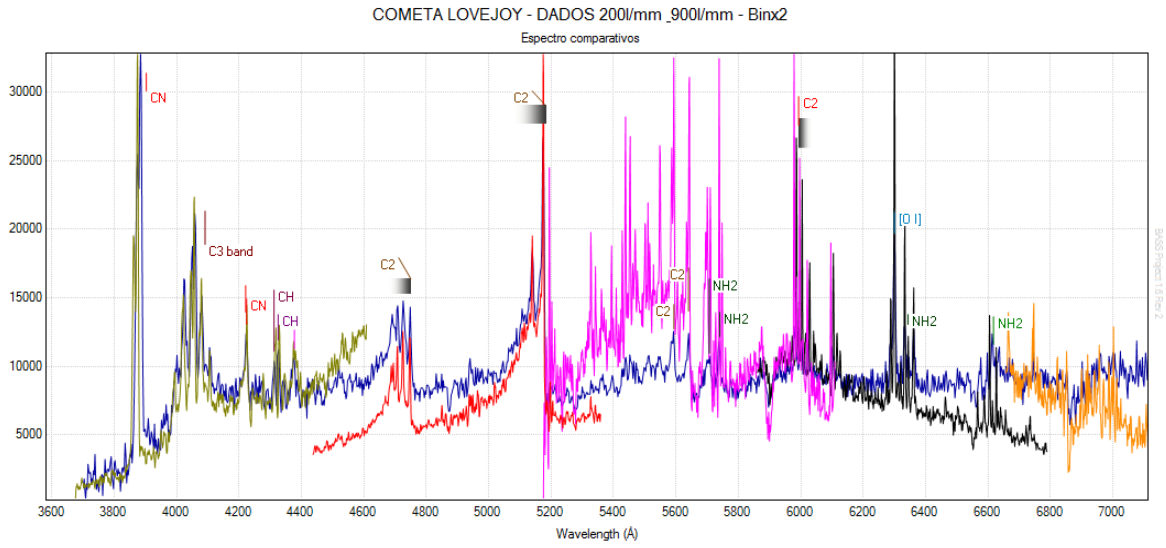

References

Huebner, W. F., Benkho, J., Capria, M.-T., Coradini, A., De Sanctis, C., Orosei, R., Prialnik, D. 2006, "Heat and Gas Diffusion in Comet Nuclei".

Cremonese1, G., Capria, M. T., De Sanctis, M. C., "Catalog of the emission lines in the visible spectrum of comet 153P/Ikeya-Zhang".

Brobovnikoff, N. T. 1925d, "Note of the spectrum of the periodic comet Temple-2".

Brown, M. E., Bouchez, A. H., Spinrad, H., Johns-Krull, C. M. 1996, "A high-resolution catalog of cometary emission lines". The Astronomical Journal, volume 112, number 3.

Churyumov1, K. I., Lukyanyk1, I. V., Chubko1, L. S., Kleshchonok1, V. V., Berezhnoy, A. A., Chavushyan, V. H., Sandoval, L., Palma, A. 2002, "Exploration of Spectra of Periodic Comet 153p/Ikeya–Zhang".

Hobbs, L. M., Thorburn, J. A., Oka, T., Barentine, J., Snow, T. P., York, D. G. 2004, "Atomic and Molecular Emission Lines from the Red Rectangle".

Biver, N., "Cometary Spectroscopy", LESIA, UMR8109 du CNRS, Observatoire de Paris-Meudon.

Goraya, P. S., Saneal, B. B., Rautela, B. S. 1984, "The spectrum of the periodic comet Encke".

Churyumov, K. I., Lukyanik, I. V., Afanasiev, V. L., Moisseev, A.V. 2001, "Exploration of the comet 19P/Borrelly, obteined with the MPFS and scorpio of 6M telescope".

Mallama, A. 2015, J. Amer. Assoc. Var. Star Obs. 43, 64-66
http://www.aavso.org/media/jaavso/3075_3.pdf).